nature climate change

Article

https://doi.org/10.1038/s41558-023-01715-3

Sensitivity of Arctic CH_4 emissions to landscape wetness diminished by atmospheric feedbacks

In the format provided by the authors and unedited

Table of Contents

Simulations

Coupled MPI-ESM Simulations

The coupled simulations use two setups of the land surface model that assume different degrees of ”wetness” in the northern permafrost-affected grid cells, namely a Wet and an increasingly Dry setup. Here, wetness does not merely refer to the saturation of the soils, but all elements of the terrestrial hydrological cycle are assumed to be consistent with conditions that favour either a high or a low soil water content and, more importantly, a large or a small spatial extent of waterlogged soils and inundated areas. Thus, the ”Wet” setup assumes high infiltration rates combined with a good hydrological storage capability, which stems from a strong inhibition of the drainage fluxes in the presence of soil ice. Furthermore, the Wet setup assumes a low resistance with respect to bare soil evaporation and transpiration, even though this appears counteractive as the resulting higher evapotranspiration rates initially reduce the soil moisture content. However, the increase in evapotranspiration is largely balanced by higher precipitation rates – hence the net effect on the soil water content is negligible – with the latter resulting in a larger wetland area due to increased ponding. Furthermore, larger transpiration and bare soil evaporation rates reduce the evaporation from inundated areas – hence lead to a larger spatial extent of waterlogged soils – because more of the atmospheric moisture demand is satisfied by fluxes from the vegetation and from non-inundated bare-soil areas.

In contrast the ”Dry” setup is based on dynamical parametrizations, which facilitate the desiccation of the soils in the northern permafrost regions. This setup assumes that the characteristics of the soil hydrology are determined by the presence of near-surface permafrost and change when the latter is degraded. All grid cells start with the parametrizations of the Wet setup and the configuration is maintained as long as the model simulates permafrost in the upper 3 m of the soil. However, the parametrizations switch from Wet to Dry – the latter being characterized by lower infiltration rates, a poor soil water retention, due to a reduced drainage-inhibition at cold temperatures, large runoff and drainage rates and a high resistance with respect to evaporation and transpiration – whenever the previous year’s maximum thaw depth in the grid-cell exceeds a depth of 3 m. For the high emission scenario considered in this study, the majority of the grid cells north of 60°N transitions from Wet to Dry during the 21st century, with the Dry simulation becoming increasingly different from the Wet simulation.

In the Wet setup, the high water retention ability of the soils is achieved by assuming that the presence of ice does not only inhibit the vertical fluxes of water but also the lateral drainage of the soils, so that the latter is only possible from fully saturated layers. Additionally, all supercooled water is assumed to be bound to the mineral particles and unable to move through the soil matrix. In contrast the Dry simulation assumes that – once the near surface permafrost is degraded – lateral drainage is possible even if the soils are not fully saturated and the respective fluxes are calculated using the model’s standard drainage formulations. Furthermore, supercooled water is treated in the same way as liquid water above the freezing point and – unless the underlying pore-spaces are largely occupied by ice – can move vertically through and drain from the soil. With respect to infiltration the Dry setup assumes that at least 20 % of all precipitation, snowmelt, throughfall and stemflow run off at the surface regardless of the saturation of the soil and the orography of the grid box. Only the remaining 80 % are divided into surface runoff and infiltration according to the model’s standard infiltration scheme. In the Wet simulations all water that reaches the surface can potentially infiltrate if the soil conditions and the orography allow it. Finally, the Dry simulation assumes a high resistance with respect to transpiration and evaporation from bare-soil areas by increasing the values of the parameters representing the maximum root zone soil moisture and top layer soil moisture by the additional pore space of an organic top layer. In contrast the Wet simulation assumes a low resistance – by using the model’s standard parameters – which leads to a higher bare-soil- and lower wetland evaporation.

It should be noted that the design of the setups is – to a certain degree – arbitrary and the differences between the Wet and Dry simulations do not cover the complete uncertainty-range included in the parametrizations of JSBACH’s soil hydrology scheme. Instead our aim was to limit the differences between the simulations to the range of ”typical” inter-model differences both with respect to the hydrological response of the land surface model to given atmospheric conditions but also with respect to the resulting climate feedbacks[1]. Finally, the adapted code is only executed in those grid-cells in the Artic and subarctic region, that are affected by permafrost, while in the rest of the world the parametrizations of the standard model are used. Here, the seperation in permafrost and non-permafrost grid-cells is not based on the permafrost extent as simulated by JSBACH – as this differs between setups – but on the observed, present-day extent using data from the Northern Circumpolar Soil Carbon Database[2].

The general setup of the coupled simulations uses a 450-second timestep for the atmospheric- and the land component, while the ocean model is run with a 2700-second timestep. The horizontal resolution in the atmosphere and over land is T63 (1.9° × 1.9°) – which corresponds to a grid-spacing of about 200 km in tropical latitudes – and GR15 (1.5° × 1.5°) in the ocean, corresponding to 160 km in the tropics. The atmosphere has a vertical resolution of 47 levels reaching up to 0.1 hPa, which is a

height of about 80 km, while the ocean model uses 41 vertical layers reaching to a depth of up to 5000 m. The land-surface is resolved by 18 sub-surface layers that extend to a depth of about 160 m – 11 of which are used to represent the top 3 m of the soil column – which is a higher resolution than the standard setup which uses 5 layers reaching to a depth of roughly 10 m. In the simulations, the water- and energy cycles of the MPI-ESM-components are fully coupled, while the simulated carbon fluxes from the land and the ocean have no effect on the atmospheric greenhouse gas concentrations. Instead we assume that variations in the natural greenhouse-gas fluxes will be balanced by adjustments to the athropogenic emissions, so that the atmospheric concentrations follow the Shared Socioeconomic Pathway 5 and the Representative Concentration Pathway 8.5 (SSP5-8.5)[3]. Here, the scenario starts with pre-industrial atmospheric CO_2 concentrations of about 280 ppmv, which increase to about 400 ppmv by the year 2014. For the future period, SSP5-8.5 assumes a high GHG emission trajectory, targeting a radiative forcing of 8.5 W m^{-2}, and assumes the atmospheric CO_2 concentrations to increase to about 1100 ppmv in the year 2100.

The Wet simulation starts in the year 1800, with the atmosphere and the ocean being initialized using pre-industrial control simulations with the standard MPI-ESM, which were performed as part of the CMIP6 deck experiments[4]. With respect to the land surface, the CMIP6 setup differs to the present model version and the terrestrial states cannot be initialized in the same manner. Here, we used a temperature approximation – based on the surface temperature – to initialize the soil temperature and assumed all soils layers to be close to saturation – that is at 95% of the maximum water holding capacity. Starting from this state, we ran JSBACH in standalone-mode for 200 years, with the atmospheric forcing data derived from the MPI-ESM pre-industrial control simulations. During this period the soil temperatures, soil water and ice content, and the vegetation adjust to the prescribed atmospheric conditions, allowing us to use the final states to initialize the fully coupled simulations. The Wet and the (increasingly) Dry trajectory begin to diverge when the near-surface permafrost disappears from the grid cells that are at present underlain by permafrost. We assume that, in the latitudes north of 60°N, this is largely the case only after the beginning of the 21st century, allowing us to initialize the Dry simulation from the states that are simulated for the Wet simulation in the year 1950.

JSBACH standalone simulations

The model version that is used for the standalone simulations is described in detail in de Vrese et al. (2021)[5]. For the present investigation, however, we made two important changes regarding the parametrizations of the soil physics routines. One change being that the present model version includes the same flexibility with respect to the soil hydrology as the version used in the coupled simulations, allowing us to run the model with Wet and increasingly Dry conditions in the permafrost affected grid-cells. Additionally, the effect of soil organic matter on the thermophysical- and hydrological soil properties is only taken into consideration in the top soil layer, even though the organic matter concentrations are explicitly simulated up to a depth of 3 m. This was done in order to ensure that the physical processes in the standalone simulations are consistent with those in the coupled simulations, where the the soil organic matter is merely represented by an organic top-soil layer. Furthermore, we used different values for two of the key parameters in the methane module, namely the Q10 factor and the reference temperature. In the present study we use Q10 factors of 3.0 and 3.5 (see below) and a reference temperature of 284 K, while in de Vrese et al. (2021) a Q10 of 1.5 and a reference temperature of 295 K were used. With these parameter-settings the model simulates present-day wetland emissions of around 10 - 20 Tg(CH4) in the region between 60° and 90° North (see Supplementary Fig. SF6 - SF10), which is in good agreement with other model- and observation-based estimates[6].

As stated above, the reason for combining coupled and standalone simulations in our investigation was to be able to vary some the uncertain biophysical assumptions in the model without substantially increasing the computational demand. One of the key uncertainties is strength of nitrogen limitations in high-latitude ecosystems. The concept of JSBACH's nitrogen cycle is described in detail in Parida (2011)[7] and was implemented in its present form by Goll et al. (2017)[8]. In the implementation, the nitrogen inputs into the terrestrial ecosystem stem from biological nitrogen fixation and atmospheric depositions. With respect to losses from the mineral nitrogen pool the model accounts for leaching and denitrification. As in most global models, JSBACH represents nitrogen fixation as a function of NPP[9] using an empirical relationship based on a compilation of site measurements[10], while the deposition flux is a prescribed forcing. For denitrification the model assumes a maximum rate of 0.02 % per day which is reached under unstressed conditions[11] and down-scaled according to a simulated water stress factor. Leaching is a function of the dissolved nitrogen and the rate with which water drains from the soil. Here, the fraction of mineral nitrogen in soil solutions is one of the main tuning parameters and in the present implementation its value is 0.1, which is comparable to fractions used in other models[12] as well as to those found by observation-based studies[13].

The vegetation takes up nitrogen from the soil mineral nitrogen pool, with the nitrogen being allocated to the woody and green plant tissue according to fixed N : C ratios. Here, nitrogen limitations – that is nitrogen-availability induced limitations to NPP – are implemented by calculating the actual productivity by down-scaling potential NPP using the ratio of available

nitrogen : required nitrogen. Upon leaf shedding, nitrogen is transferred from the green plant tissue to leaf litter pools, while the wood pool has a fixed turnover time, with nitrogen being transferred to woody litter pools. Microbial activity, as calculated by the YASSO model, mediates the transfer of nitrogen from the litter pools to the soil humus pool. As the N : C ratio of the humus pool is larger than the N : C ratios of the green and woody litter pools, additional nitrogen from the soil mineral nitrogen pool is required (immobilization). Here, nitrogen limitations act on the decomposition of litter in the same way they act on NPP – down-scaling the potential decomposition rate using the ratio of available nitrogen : required nitrogen – so that no assumption about the relative competitive strengths of microbial and plant consumption is being made. When the organic matter in the humus pool decomposes the respective nitrogen is returned to the soil mineral nitrogen pool (mineralization).

For our simulations with an active nitrogen cycle, we did not change the respective parametrizations from the way described in Goll et al. (2017)[8]. However, the present model version produces nitrogen limitation that are substantially higher than those in the standard model. In the fully adapted model, the nitrogen limitations lower the primary productivity and soil respiration rates by up to 35% while the vegetated fraction is reduced by up to 20%. In contrast, these limitations merely amount to a few percent in the standard model. This increase in nitrogen limitations is the results of model improvements, mainly including the phase change of water in the soil – which has a strong effect on the amount and timing of drainage hence on nitrogen leaching – and by calculating the decomposition of soil organic mater using soil temperature and soil moisture rather than surface temperature and precipitation. The latter reduces the (net) mineralization flux especially at the beginning of the century because the low ground temperatures result in decomposition rates of the humus pool that are much lower than the litter flux into the soil. Here, the nitrogen limitations that the adapted model estimates in the high latitudes are actually not (substantially) higher than other model-based estimates, e.g. the Community Land Model produced plant type specific (NPP) limitation factors of up to 30% for Arctic vegetation[14] and using LPJml, the simulated GPP in boreal and tundra regions is reduced by up to 40% by nitrogen limitations[15]. Furthermore, these limitations fit (at least qualitatively) with observation-based studies that indicate that high-latitude productivity could be significantly nitrogen limited[16]. Thus, "high nitrogen limitations" is to be understood merely relative to the nitrogen limitations that the standard JSBACH model produces. Nonetheless, the role of the nitrogen limitations is highly uncertain, especially in the case of thawing permafrost soils. Consequently, we did not attempt to find a best-estimate setting for the respective parameters in the model, but instead performed two sets of simulations, one with the standard parameter values in the nitrogen module and one in which nitrogen limitations are not taken into consideration (see supplementary materials Fig. SF6).

A second important source of uncertainty is the size and vertical distribution of the initial soil carbon pools, which have built up in the frozen soils during and since the last glacial period[17–19]. To initialize the soil carbon concentrations within the first two meters of the soil, we use the vertically resolved, harmonized soil property values from the WISE30sec dataset[20], which are based on soil profiles provided by the WISE project[20,21] and have the advantage of being consistent with the FAO soil units which were used to derive the soil properties for the JSBACH model[22,23]. For depth below two meters we use data from the Northern Circumpolar Soil Carbon Database[2]. However, this initialization using observation-based soil carbon concentrations is not without problems.

One problem is a potential inconsistency between the observed soil carbon concentrations, the simulated climate conditions and the state of the vegetation, which was initialized using the output of a control simulation with the standard version of the MPI-ESM. To minimize these inconsistencies we initialize the experiments with the observation-based, present-day carbon soil pools but start the simulations in the year 1850 at the end of the pre-industrial period. In the high northern latitudes this allows the carbon concentrations within the (simulated) active layer to adapt to the simulated climate conditions and the state of the vegetation during the historical period, while the perennially frozen regions of the soil conserve the observed carbon concentrations.

Another problem arises because there are regions in the high latitudes where the observed carbon pools are not only inconsistent with the simulated climate but also with the standard soil depths used by the model. The main reason for this is the high spatial variability in the real-world soil depths, which cannot be represented at the coarse resolution of the model. This inconsistency results in large amounts of the observed organic matter being located in parts of the ground that the model considers to be below the bedrock boundary. When limiting the organic matter to the top- and subsoil – the soil above the bedrock – of the standard setup, the soils in the northern high latitudes are initialized with as little as $\approx$ 650 GtC in the uppermost 3 m of instead of the observed $\approx$ 1000 GtC. Consequently, limiting the initial carbon pools to the observed organic matter concentrations within JSBACH's standard soil depths includes the risk of substantially underestimating the effect of increasing temperatures on the soil carbon release. To partly mitigate this issue, we performed two sets of standalone simulations, with one set using the standard soil depths, while the other uses a soil configuration with extended soil depths[5,24,25]. For the simulations

using the standard soil depths, we increased the organic matter concentrations in the layers above the bedrock boundary – to 858 GtC. Hence, the total soil organic matter content better matches the observations, while the near-surface concentrations are overestimated. The extended soil depths in the second set of simulations allow storing more organic matter – up to ≈ 800 GtC – in the Arctic and subarctic permafrost soils. Thus, the initial soil carbon concentrations are already closer to the observation based values and with an up-scaling – here we increased the soil carbon concentrations to 931 GtC – both the total soil organic matter content and the concentrations better match the observations. However, these soil depths do not represent the bedrock boundary appropriately at coarse resolutions, which affects the behaviour of the model in parts of the northern high latitudes. Here, one particular issue with respect to the methane emissions is the vertical position of the water table. At given precipitation and evapotranspiration rates, the water table is often lower when the soil-bedrock boundary is lower, which means that the TOPMODEL approach estimates a smaller fraction of the grid cell to feature fully water saturated soils. Additionally, the soil depth has an important impact on the potential rooting depths, the water availability and -stress – which is approximated by the relative saturation of the root-zone – and, consequently, on the vegetation distribution. Here, deeper soils predominantly result in a lower grass cover, with a significant effect on the plant mediated CH_4 transport and oxidation rates. Consequently, the model often simulates lower CH_4 emissions for the same climatic conditions, despite higher initial soil carbon concentrations and comparable carbon inputs (see supplementary materials Fig. SF7).

One of the largest sources of uncertainty stems from the parameter uncertainty involved in simulating soil methane production, transport and oxidation. And while the methane emissions simulated for the present day can be compared to observation based estimates and other models[6], this is vastly more difficult for the individual factors that determine the fluxes at the surface – that is the same net emissions can be achieved for very different combinations of methane production and oxidation or for different combinations of diffusive and plant mediated transport. Thus, rather than performing one set with a best-estimate parameter setting, we performed two sets of extreme simulations: One characterized by high methane production and oxidation rates, where the largest fraction of the emissions at the surface stems from plant-mediated transport and another set with lower production and oxidation rates and a reduced plant mediated transport. For the high-production-high-oxidation simulations we assume a fraction of anaerobically mineralized C atoms becoming CH_4 of 0.4 and a Q10 for the methane production of 3.0, while the low-production-low-oxidation set assumes 0.2 and 3.5 respectively. With respect to oxidation, the high-production-high-oxidation simulations assume a Q10 of 1.9 and a maximum oxidation rate of $1.25e^{-5}$, while the low-production-low-oxidation set assumes 3.0 and $1.25e^{-6}$. With respect to the plant mediated transport, the high-production-high-oxidation-simulations use the parameter values as described in Riley et al. (2011)[26], while the low-production-low-oxidation simulations apply an additional scaling factor of 0.1 to the transport rates.

In addition to these simulations we performed another three sets of simulations that increase the projected wetland area under given climate conditions. These additional simulations, however, were only performed for the Wet scenario (see supplementary materials Fig. SF9 and SF10). The resulting changes in the simulated wetland area are minor – on average around 1% of the grid-box area – but they can have a pronounced effect on the simulated methane emissions, especially at the end of the 21st century, if they occur in regions with high soil carbon concentrations. As described above, the offline version of the model uses two schemes to estimate the fraction for two wetland components. The first scheme simulates the effect of ponding – the formation of wetlands because water cannot infiltrate fast enough and pools at the surface, while the second scheme accounts for inundated areas that form in highly saturated soils due to low drainage fluxes. Here, both schemes calculate the inundated fraction based on the subgrid-scale orography, assuming that wetlands predominantly form in the flatter, low-laying parts of the grid-cell. Thus, when combining the wetland areas of the two schemes, we assume that these refer to the same part of the grid-cell and use the larger of the two values as the overall wetland area. But for one of the additional sets of simulations we changed the underlying assumption and calculate the overall wetland area by adding the grid-cell fraction of the two wetland components. However, it should be noted that this increases the overall wetland area only slightly, because the two wetland components have very different seasonal dynamics and the temporal overlap of the two is comparatively small. The wetland area due to ponding shows a pronounced peak after the snowmelt season during spring but rapidly declines in early summer, whereas the wetlands due to low drainage fluxes dominate during summer and fall, when the water from the snowmelt flux has largely infiltrated, the ice in the ground has partly melted and there is a lot of liquid water in the soils.

For another set of simulations with the Wet setup, we used a highly synthetic configuration that targets reduced evapotranspiration rates which remove only a little water from the soil. As stated above, the Wet setups generally assumes a low resistance with respect to bare soil evaporation and transpiration which initially reduces the soil water content. Here, preliminary simulations showed that the water loss is offset by increased precipitation, with the overall effect on the soil water content being negligible. Yet in order to maximize the simulated wetland area under given climate conditions we calculated the amount of water that is removed by evaporation and transpiration based on a high resistance similar to the configuration of the Dry setup,

while calculating the latent heat-flux in the surface energy balance – hence the evaporative cooling at the surface – based on the low resistance that are used in the majority of the Wet simulations. This was done in order to simulate near surface temperatures that are consistent with the atmospheric forcing, but it should be noted that the approach violates the water balance of the model and constitutes the least plausible of the model setups of the present study.

Finally, the last set of simulations with the Wet setup, combines the above approaches to maximize the wetland are – that is adding the grid-cell fractions of the two wetland components rather than taking the maximum of the two and using different assumptions for the calculation of evapotranspiration and the latent heat flux. Thus, overall we performed 8 standalone simulations for the Dry trajectory – high and no nitrogen limitations combined with the standard and increased soil depths (and low and high initial carbon pools) and with high and low methane production and oxidation rates – and 32 simulations for the Wet scenario – high and no nitrogen limitations combined with standard and deep soils, with high and low methane production and oxidation rates and with the four different approaches to estimate the wetland extent.

#	Config.	Forcing	Infil.	Drain. lat.	Supercool	ET (water)	LE (energy)	Wetlands	N lim.	Soil depth & c. pools	CH_4 Prod. & Oxid	Fig.	Ref.
1	ESM (Dry)		80	↑	moible	↓	↓	WEED	↓	↓	X	2, SF1	[1]
2	ESM(Wet)		100	↓	immob.	↑	↑	WEED	↓	↓	X	2, SF1	[1]

Supplementary Table ST1. Overview of key setup-features of fully coupled MPI-ESM simulations: Shown is the general configuration of the model (”Config.”) and, for LSM-only runs, the table further indicates which coupled simulation provided the forcing (”Forcing”). ”Infil.” gives the fraction [%] of the outflow of the surface reservoir that can potentially infiltrate and ”Drain lat.” indicates if lateral drainage is impeded in the presence of soil ice, with upward arrows indicating no-impedance (note that percolation is impeded in any case). ”Supercool” indicates whether water that remains liquid at sub-zero temperatures can move through the soil. ”ET (water) / LE (energy)” indicate the resistance to bare soil evaporation and transpiration that are assumed in the calculation of the surface moisture (ET (water)) and energy fluxes (LE (energy)). Upward arrows indicate low resistances, hence large fluxes. Note that in simulations #15-22 and #35-42 there is an inconsistency between the water and energy fluxes, which was introduced to maximise the potential wetland area. ”Wetlands” indicates which approach was used to determine the maximum wetland fraction. N lim.” indicates if the setup accounts for nitrogen limitations, while ”Soil depth & c. pools” shows whether the standard soil depths (and low initial carbon pools) were used or deeper soils (and higher initial carbon pools). ”Fig.” and ”Ref.” point to the figures that use the simulations and to the publications containing the model description.

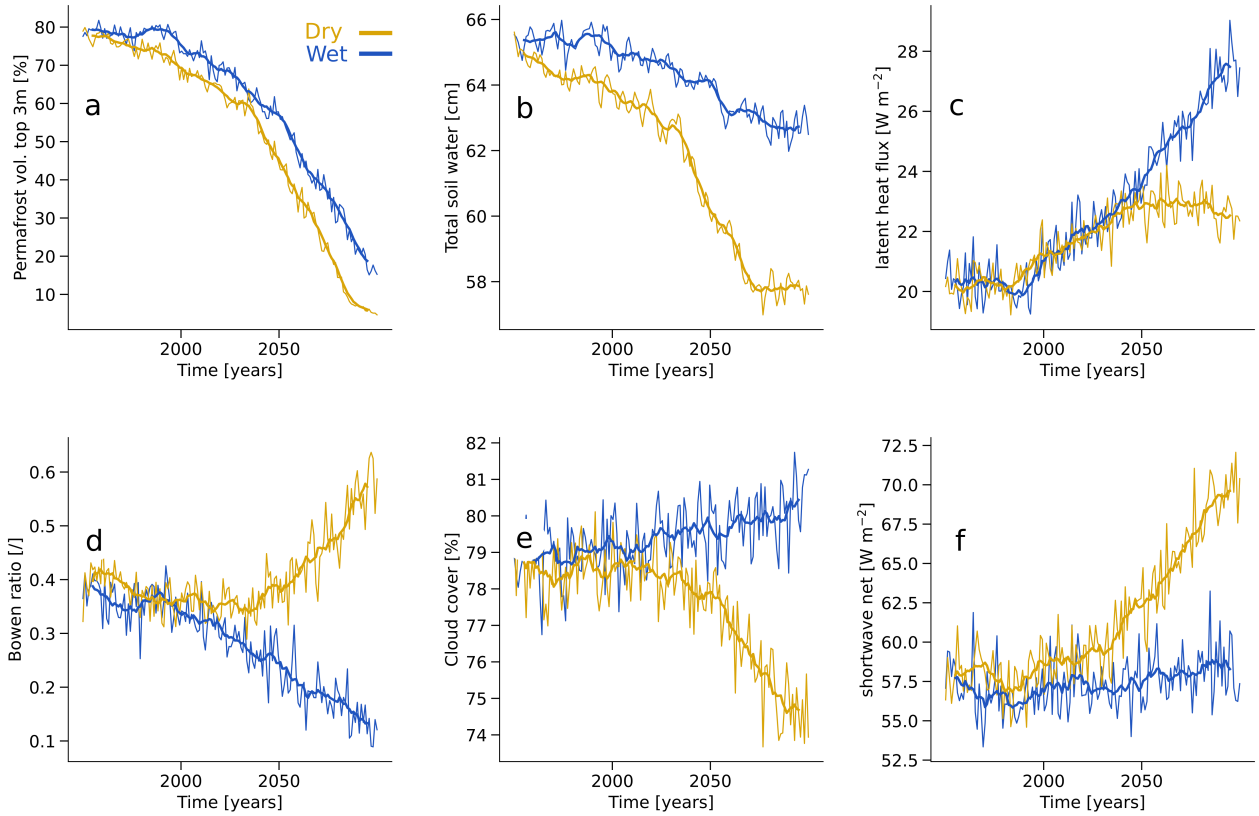

Supplementary Figure SF1. Divergence in the land-atmosphere interactions:
For the high emission scenario SSP5-8.5, the 21st-century warming results in a substantial decline in the extent and thickness of the near-surface permafrost, which reduces the total water content – that is liquid water and ice – of the Arctic and subarctic soils (a). And while the soils lose water even if drainage is strongly inhibited in the presence of ice (b), that is the Wet setup (simulation #2 in table ST1), the drying trend is much more pronounced when the ability to retain water decreases with the disappearance of the near-surface permafrost, as is the case in the Dry setup (simulation #1 in table ST1). The diverging responses to the permafrost degradation do not only affect the extent of waterlogged areas, but also the land-atmosphere interactions. While there is a mere 10 %-rise in evapotranspiration in the Dry simulation, the evapotranspiration rates in Wet increase by about a third between the years 2000 and 2100 (c). This results in a substantial divergence in the simulated Bowen ratios (d) and, consequently, increasingly large differences in the atmospheric relative humidity. In the Wet scenario there is a strong evaporation-precipitation feedback and precipitation rates increases by almost 150 mm year^{-1} during the 21st century (main manuscript Fig. 1a). In contrast precipitation increase by merely 75 mm year^{-1} when the soils show a more pronounced drying in response to permafrost thaw. The additional evaporative cooling in the Wet simulations and the resulting higher atmospheric humidity also allows a comparatively stable cloud cover to be maintained, while the Dry simulation exhibits a substantial decline in the cloudiness in the northern permafrost regions (e). The clouds, in turn, determine the incoming shortwave radiation at the surface and, when additionally accounting for differences in the surface reflectively (mainly resulting from differences in the vegetation cover) – the absorbed shortwave radiation increases by roughly 20 % in Dry, while there is almost no increase in the Wet simulation (f). In combination with the additional evaporative cooling, this has a strong impact on the surface energy budget and by the end of the century the Wet simulation is on average about 2°C cooler than the Dry simulation (main manuscript Fig. 1b), while the near-surface permafrost volume is about 10% higher.

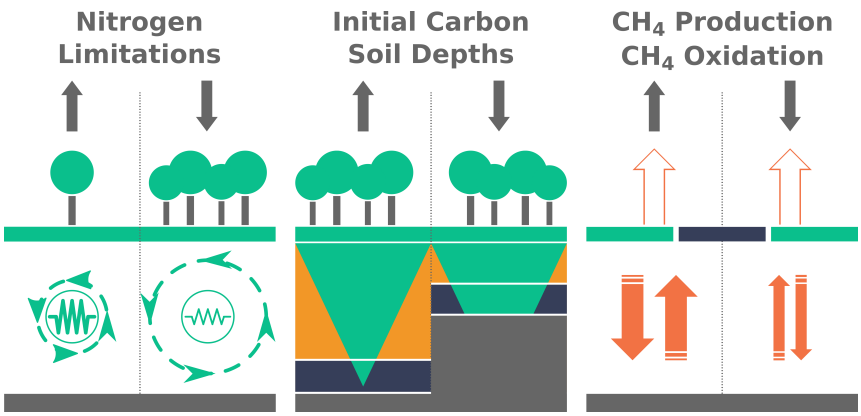

Supplementary Figure SF2. Schematic overview of key uncertainties addressed by different sets of JSBACH standalone simulations:
Left panel - In the standard JSBACH version, nitrogen limitations reduce the primary productivity in the high latitudes by a few percent, while in the present model version, the NPP reduction can be as high as 35% (during the pre-industrial period) which can lead to a reduction in vegetation cover of up to 20%. Rather than performing a simulation with best-estimate parameters we conducted one set of simulations (↑) with the high nitrogen limitations resulting from using our adjusted JSBACH version with the standard parameter setting of the nitrogen model and one set (↓) that does not account for nitrogen limitations. For a comparison of the two sets of simulations see Fig. SF6.
Center - Due to the coarse resolution of our model, it is impossible to initialize simulations with the standard soil depths using observation-based soil carbon pools. Here, we performed one set of simulation with deeper soils (↑), allowing us to initialize the simulations with carbon pools that are closer to the observation-based estimates and one set of simulations (↓) with the standard soil depth, where we up-scaled the carbon concentrations at the surface but still initialized the model with a lower soil organic matter content. For a comparison of the two sets of simulations see Fig. SF7.
Right panel - Estimates of the high latitude methane emissions are very uncertain[6], and the uncertainty increases for the processes that determine the net fluxes, such as methane production and methane oxidation. To address this uncertainty, we conducted two sets of simulations, which resulted in comparable present-day emissions. In one set (↑) we assumed a high methane production and oxidation in the soil, while the second set (↓) assumes a low methane production and oxidation rates (and a low plant mediated transport). For a comparison of the two sets of simulations see Fig. SF8.

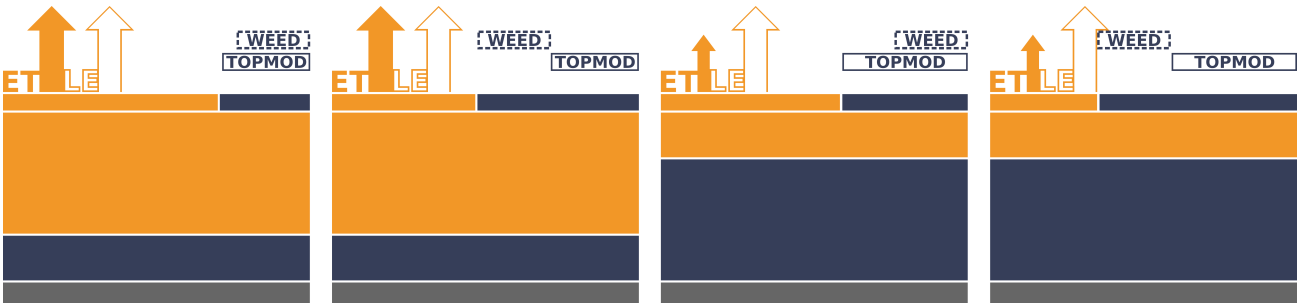

Supplementary Figure SF3. Approaches to maximise the wetland area in the Wet simulations:
Left panel - In the Dry simulations as well as in the first set of Wet simulations, the estimation of the bare soil evaporation is consistent with the calculation of the latent heat flux and the wetland area is determined as the maximum of the areas estimated by the WEED scheme and the TOPMODEL-based approach.
Center left - In a second set of Wet simulations the wetland area is calculated by adding the areas estimated by the WEED scheme and the TOPMODEL-based approach.
Center right - A third set of Wet simulations uses an idealized setup in which the calculation of the evaporative cooling – that is the latent heat flux in the surface energy balance – is based on low resistances, while the amount of evaporated water is estimated based on a high resistance. The approach allows to maintain surface temperatures that are consistent with the atmospheric forcing, while removing only little water from the soil. This results in a higher soil water content – and a larger wetland area estimated by the TOPMODEL – but violates the water balance.
Right panel - In the fourth set of Wet simulations the wetland area is maximized using a combination of the above two approaches. For a comparison see Fig. SF9 and SF10.

#	Config.	Forcing	Infil.	Drain. lat.	Supercool	ET (water)	LE (energy)	Wetlands	N lim.	Soil depth & c. pools	CH_4 Prod. & Oxid	Fig.	Ref.
3	LSM-only	Dry	80	↑	moible	↓	↓	max(WEED,TOPM)	↓	↓	↑	3-4,SF6-SF10	[1,5]
4	LSM-only	Dry	80	↑	moible	↓	↓	max(WEED,TOPM)	↓	↑	↑	3-4,SF6-SF10	[1,5]
5	LSM-only	Dry	80	↑	moible	↓	↓	max(WEED,TOPM)	↑	↓	↑	3-4,SF6-SF10	[1,5]
6	LSM-only	Dry	80	↑	moible	↓	↓	max(WEED,TOPM)	↑	↑	↑	3-4,SF6-SF10	[1,5]
7	LSM-only	Wet	100	↓	immob.	↑	↑	max(WEED,TOPM)	↓	↓	↑	3-4,SF6-SF10	[1,5]
8	LSM-only	Wet	100	↓	immob.	↑	↑	max(WEED,TOPM)	↓	↑	↑	3-4,SF6-SF10	[1,5]
9	LSM-only	Wet	100	↓	immob.	↑	↑	max(WEED,TOPM)	↑	↓	↑	3-4,SF6-SF10	[1,5]
10	LSM-only	Wet	100	↓	immob.	↑	↑	max(WEED,TOPM)	↑	↑	↑	3-4,SF6-SF10	[1,5]
11	LSM-only	Wet	100	↓	immob.	↑	↑	WEED+TOPM	↓	↓	↑	3-4,SF6-SF10	[1,5]
12	LSM-only	Wet	100	↓	immob.	↑	↑	WEED+TOPM	↓	↑	↑	3-4,SF6-SF10	[1,5]
13	LSM-only	Wet	100	↓	immob.	↑	↑	WEED+TOPM	↑	↓	↑	3-4,SF6-SF10	[1,5]
14	LSM-only	Wet	100	↓	immob.	↑	↑	WEED+TOPM	↑	↑	↑	3-4,SF6-SF10	[1,5]
15	LSM-only	Wet	100	↓	immob.	↓	↑	max(WEED,TOPM)	↓	↓	↑	3-4,SF6-SF10	[1,5]
16	LSM-only	Wet	100	↓	immob.	↓	↑	max(WEED,TOPM)	↓	↑	↑	3-4,SF6-SF10	[1,5]
17	LSM-only	Wet	100	↓	immob.	↓	↑	max(WEED,TOPM)	↑	↓	↑	3-4,SF6-SF10	[1,5]
18	LSM-only	Wet	100	↓	immob.	↓	↑	max(WEED,TOPM)	↑	↑	↑	3-4,SF6-SF10	[1,5]
19	LSM-only	Wet	100	↓	immob.	↓	↑	WEED+TOPM	↓	↓	↑	3-4,SF6-SF10	[1,5]
20	LSM-only	Wet	100	↓	immob.	↓	↑	WEED+TOPM	↓	↑	↑	3-4,SF6-SF10	[1,5]
21	LSM-only	Wet	100	↓	immob.	↓	↑	WEED+TOPM	↑	↓	↑	3-4,SF6-SF10	[1,5]
22	LSM-only	Wet	100	↓	immob.	↓	↑	WEED+TOPM	↑	↑	↑	3-4,SF6-SF10	[1,5]
23	LSM-only	Dry	80	↑	moible	↓	↓	max(WEED,TOPM)	↓	↓	↓	3-4,SF6-SF10	[1,5]
24	LSM-only	Dry	80	↑	moible	↓	↓	max(WEED,TOPM)	↓	↑	↓	3-4,SF6-SF10	[1,5]
25	LSM-only	Dry	80	↑	moible	↓	↓	max(WEED,TOPM)	↑	↓	↓	3-4,SF6-SF10	[1,5]
26	LSM-only	Dry	80	↑	moible	↓	↓	max(WEED,TOPM)	↑	↑	↓	3-4,SF6-SF10	[1,5]
27	LSM-only	Wet	100	↓	immob.	↑	↑	max(WEED,TOPM)	↓	↓	↓	3-4,SF6-SF10	[1,5]
28	LSM-only	Wet	100	↓	immob.	↑	↑	max(WEED,TOPM)	↓	↑	↓	3-4,SF6-SF10	[1,5]
29	LSM-only	Wet	100	↓	immob.	↑	↑	max(WEED,TOPM)	↑	↓	↓	3-4,SF6-SF10	[1,5]
30	LSM-only	Wet	100	↓	immob.	↑	↑	max(WEED,TOPM)	↑	↑	↓	3-4,SF6-SF10	[1,5]
31	LSM-only	Wet	100	↓	immob.	↑	↑	WEED+TOPM	↓	↓	↓	3-4,SF6-SF10	[1,5]
32	LSM-only	Wet	100	↓	immob.	↑	↑	WEED+TOPM	↓	↑	↓	3-4,SF6-SF10	[1,5]
33	LSM-only	Wet	100	↓	immob.	↑	↑	WEED+TOPM	↑	↓	↓	3-4,SF6-SF10	[1,5]
34	LSM-only	Wet	100	↓	immob.	↑	↑	WEED+TOPM	↑	↑	↓	3-4,SF6-SF10	[1,5]
35	LSM-only	Wet	100	↓	immob.	↓	↑	max(WEED,TOPM)	↓	↓	↓	3-4,SF6-SF10	[1,5]
36	LSM-only	Wet	100	↓	immob.	↓	↑	max(WEED,TOPM)	↓	↑	↓	3-4,SF6-SF10	[1,5]
37	LSM-only	Wet	100	↓	immob.	↓	↑	max(WEED,TOPM)	↑	↓	↓	3-4,SF6-SF10	[1,5]
38	LSM-only	Wet	100	↓	immob.	↓	↑	max(WEED,TOPM)	↑	↑	↓	3-4,SF6-SF10	[1,5]
39	LSM-only	Wet	100	↓	immob.	↓	↑	WEED+TOPM	↓	↓	↓	3-4,SF6-SF10	[1,5]
40	LSM-only	Wet	100	↓	immob.	↓	↑	WEED+TOPM	↓	↑	↓	3-4,SF6-SF10	[1,5]
41	LSM-only	Wet	100	↓	immob.	↓	↑	WEED+TOPM	↑	↓	↓	3-4,SF6-SF10	[1,5]
42	LSM-only	Wet	100	↓	immob.	↓	↑	WEED+TOPM	↑	↑	↓	3-4,SF6-SF10	[1,5]
43	LSM-only	Dry	X	X	X	X	X	TOPM	↑	↑	↑	6	[27]
44	LSM-only	Wet	X	X	X	X	X	TOPM	↑	↑	↑	6	[27]

Supplementary Table ST2. Overview of key setup-features of JSBACH standaone simulations: Continuation of table ST1.

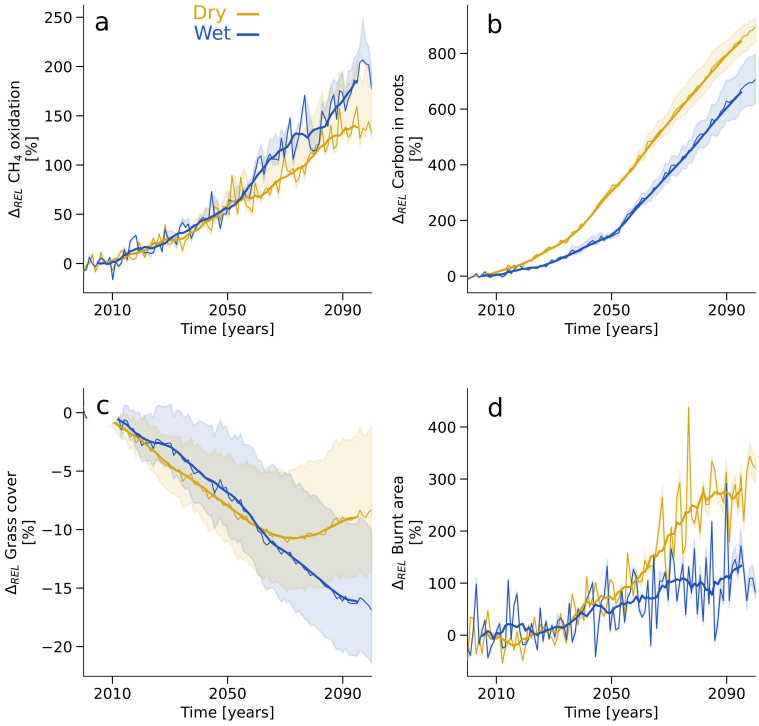

Supplementary Figure SF4. Effects of differences in vegetation dynamics:
a) Relative increase in CH_4 oxidation in the soils of the Arctic permafrost region. Blue lines show the mean of the ensemble of Wet JSBACH simulations, with the thick line indicating the 10-year running mean. The shaded area shows the spread between the ensemble minimum and maximum. Yellow colors refer to the Dry ensemble. b) Same as a, but for the root biomass. c) Same as a, but for the grass cover. d) Same as a but for burned area.
In the Wet scenario, a larger fraction of the methane produced in the deeper layers is oxidised in the oxygen-rich layers near the surface. The main reason for this is the larger fraction of methane that actually diffuses upwards, as the share of methane that is taken up by roots and consecutively transported to the surface through aerenchyma is lower. Here, the rate of methane uptake by roots is directly related to the root density, which is lower in the Wet scenario as colder conditions result in a lower net primary productivity, hence a slower build-up of below ground biomass. Furthermore, the plant mediated transport is more effective for herbaceous than woody vegetation and the grass cover exhibits a more pronounced decrease for the Wet than for the Dry simulations. Here, the partial recovery of the grass cover in the Dry simulation during the second half of the century is mainly driven by an increase in the occurrence of wild fires. The latter favour the establishment of grasses, because the build-up of stems of woody vegetation types is slow as compared to grasses, providing the latter with a competitive advantage that allows them to migrate faster into the disturbed areas[28,29]. It should be noted that the response of wildfires to a future climate change is very uncertain, though most studies suggest that, under a high emission scenario, fire-prone conditions will become much more frequent in the high latitudes[30,31]. With respect to the burned area, estimates range from roughly doubling to a fivefold increase during the 21st century[32–34]. Thus, the increase in burned area for the two scenarios is well within the range of previous estimates and, given that all fire-driving parameters are favourable in the Dry scenario – that is a higher fuel-loading, and higher temperatures combined with lower precipitation rates and dryer soils –, it is plausible that the burned area would be substantially larger in the Dry than in the Wet scenario.

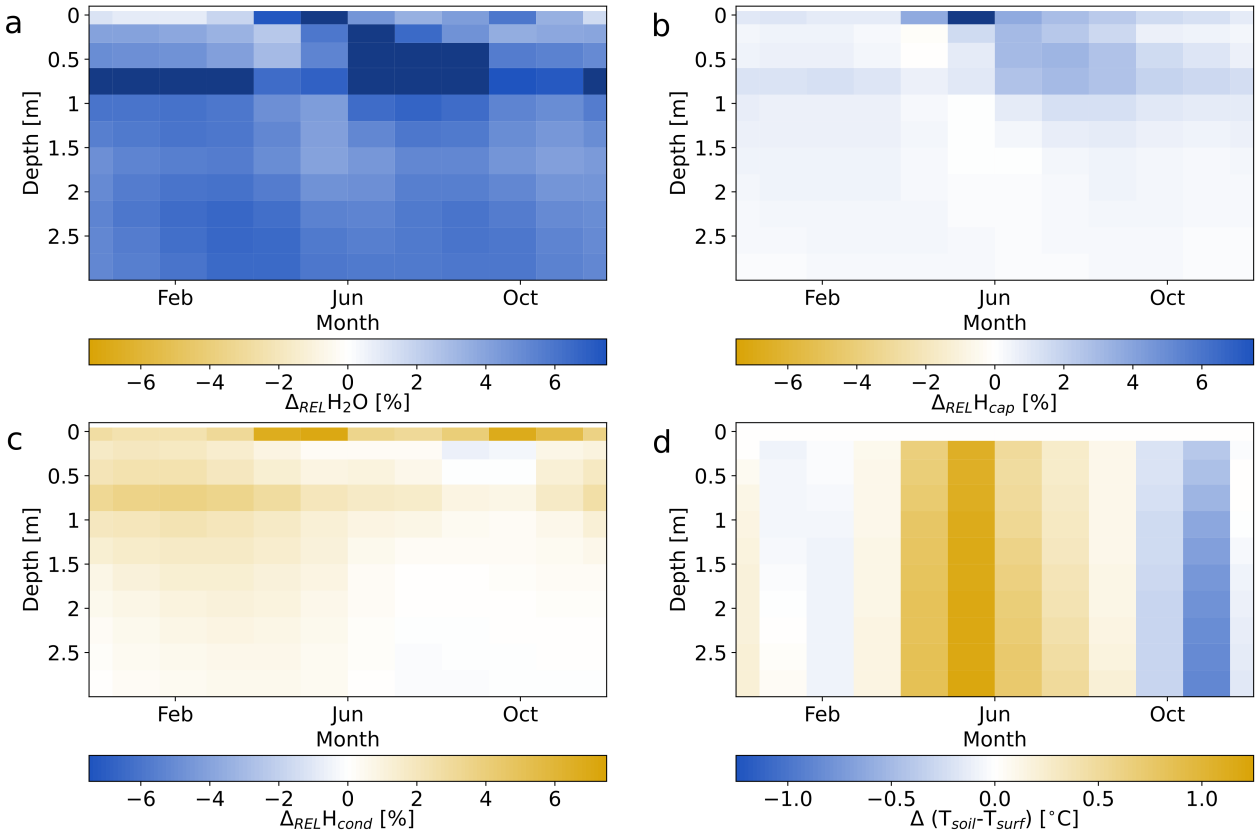

Supplementary Figure SF5. Differences in soil heat transport:
a) Relative differences in soil water content between the Wet and the Dry simulations. The figure shows the average over the Arctic region and over the period 2040 - 2059. b) Same as a, but showing relative differences in the soil heat capacity. c) Same as a, but showing relative differences in soil heat conductivity. d) Same as a but for the differences between soil and surface temperatures.

On average, the soils are more saturated in the Wet simulations than in the Dry simulations, particularly at the surface (during spring and summer) and at the bottom of the active layer (during the 2040-2059 period at around 0.75 m). As the saturation affects the thermophysical properties of the soil, both the heat capacity and the heat conductivity are higher for the Wet trajectory where a larger fraction of the pore volume is filled with water rather than air. During spring and summer, a higher heat capacity results in lower temperatures – as more energy is required to archive a given temperature increase – while the higher heat conductivity allows for a more effective downward heat transport, leading to higher temperatures at greater depths. During fall and winter, the effects are opposite, even though the effect of higher heat conductivities on the below ground temperatures is strongly muted by the presence of a snow cover, which has the same low heat conductivity in the Wet and in the Dry scenario. In our simulations, the dominant signal of different soil moisture conditions stems from the resulting differences in the heat conductivity of the organic rich surface layer, which insulates the soil against temperature fluctuations – especially when dry. With a more effective vertical heat transport, the soils in the Wet simulations warm more readily during spring and summer resulting in higher below ground temperatures relative to the temperatures at the surface (note that in absolute terms the soils in the Wet simulation are colder than those in the Dry simulation throughout the year). As a result, the annual maximum soil temperatures are much more similar in the two setups than those at the surface. With respect to soil respiration this means, that the below ground decomposition rates are also more similar than those at the surface. Hence, the soils in the Wet and in the Dry simulations loose formerly frozen soil organic matter at a rate that is much more similar than the large differences in the surface temperatures would suggest. It should be noted that in the calculation of the heat conductivity JSBACH distinguishes between frozen and unfrozen soils with the conductivity for a given saturation being lower for frozen soils than for unfrozen soils (the model uses the Johansen scheme where the heat conductivity is estimated based on a combination of the saturated and the dry conductivity weighted by the Kersten number[35]). As the soils in the Wet simulation are predominantly colder, the heat conductivity can actually be lower than the heat conductivity in the Dry simulations, despite the soil being more saturated. Furthermore, in our setups, the properties of organic matter are only taken into consideration for the surface layer (to be consistent with the coupled model which does not represent carbon on soil layers). Thus, the effect of a reduced vertical heat transport in the Dry simulation are most likely underestimated, especially in regions with large peatlands.

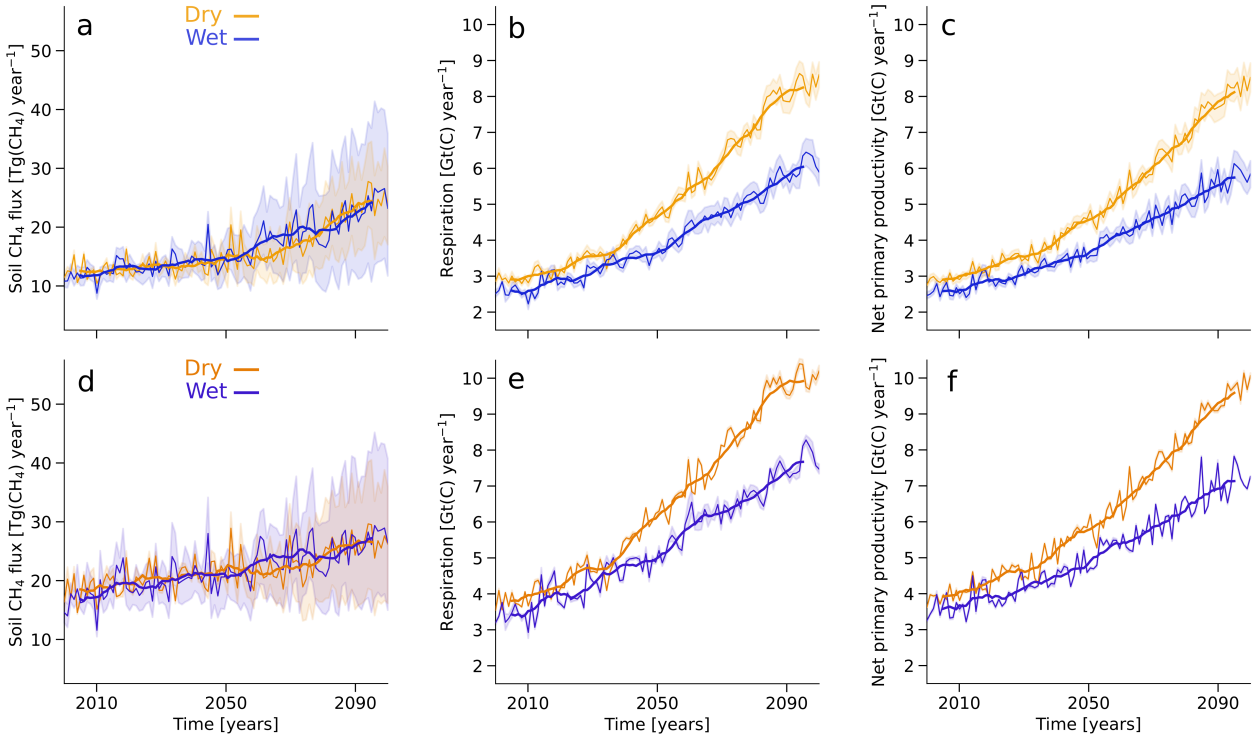

Supplementary Figure SF6. Sources of uncertainty: Nitrogen limitations
a) Simulated methane release from Arctic soils. Lines show the mean of the ensemble of Wet and Dry JSBACH simulations, with thick lines indicating the 10-year running means. The shaded areas show the spread between the ensemble minima and maxima. b) Same as a but for (oxic and anoxic) soil respiration and c) net primary primary productivity. Subfigures a - c show simulations that include nitrogen limitations (simulations #5,6,9,10,13,14,17,18,21,22,25,26,29,30,33,34,37,38,41,42 in table ST2). d) - f) Same as a - c, but for the set of simulations without nitrogen limitations (simulations #3,4,7,8,11,12,15,16,19,20,23,24,27,28,31,32,35,36,39,40 in table ST2).

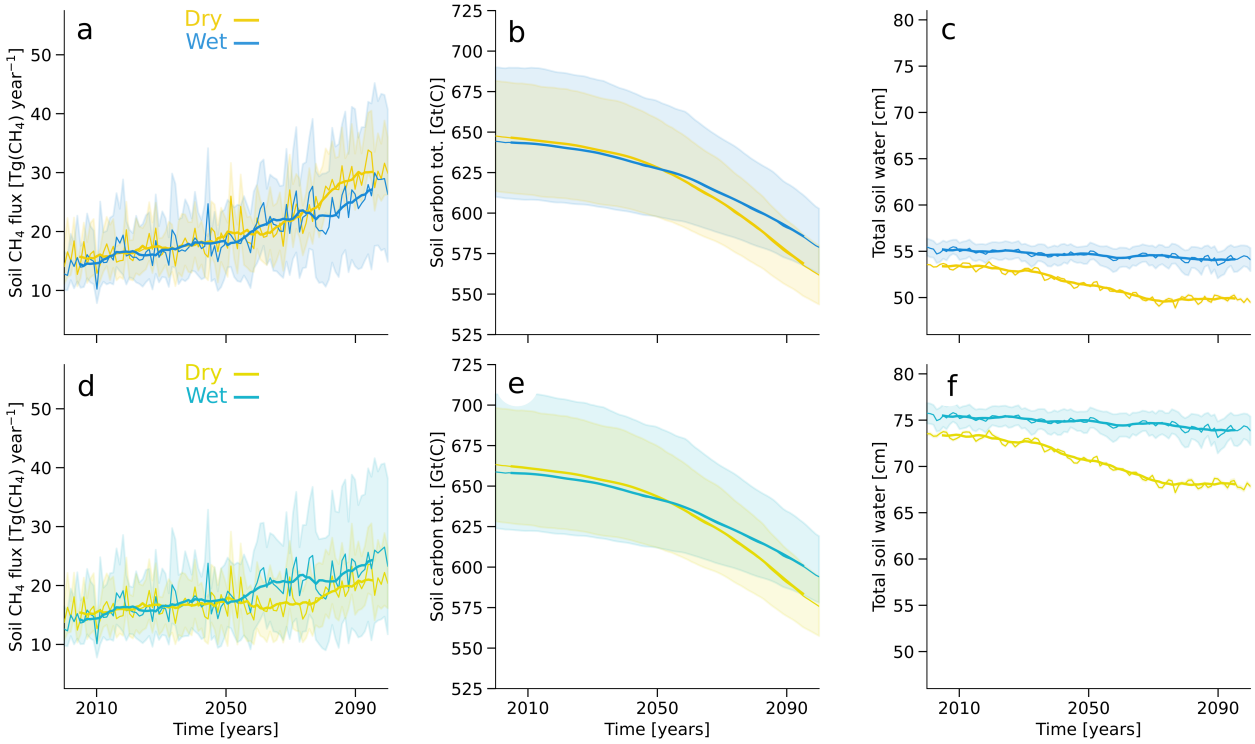

Supplementary Figure SF7. Sources of uncertainty: Soil depths (and initial soil carbon concentrations)
a) Simulated methane release from Arctic soils. Lines show the mean of the ensemble of Wet and Dry JSBACH simulations, with thick lines indicating the 10-year running means. The shaded areas show the spread between the ensemble minima and maxima. b) Same as a but for total soil carbon content and c) total soil water content. Subfigures a - c show simulations that were run with the standard soil depths and low total initial carbon pools – but overestimated soil carbon concentrations (simulations #3,5,7,9,11,13,15,17,19,21,23,25,27,29,31,33,35,37,39,41 in table ST2). d) - f) Same as a - c, but for a set of simulations with an increased soil and rooting depths and larger initial soil carbon pools and concentrations that are closer to observation-based estimates (simulations #4,6,8,10,12,14,16,18,20,22,24,26,28,30,32,34,36,38,40,42 in table ST2).

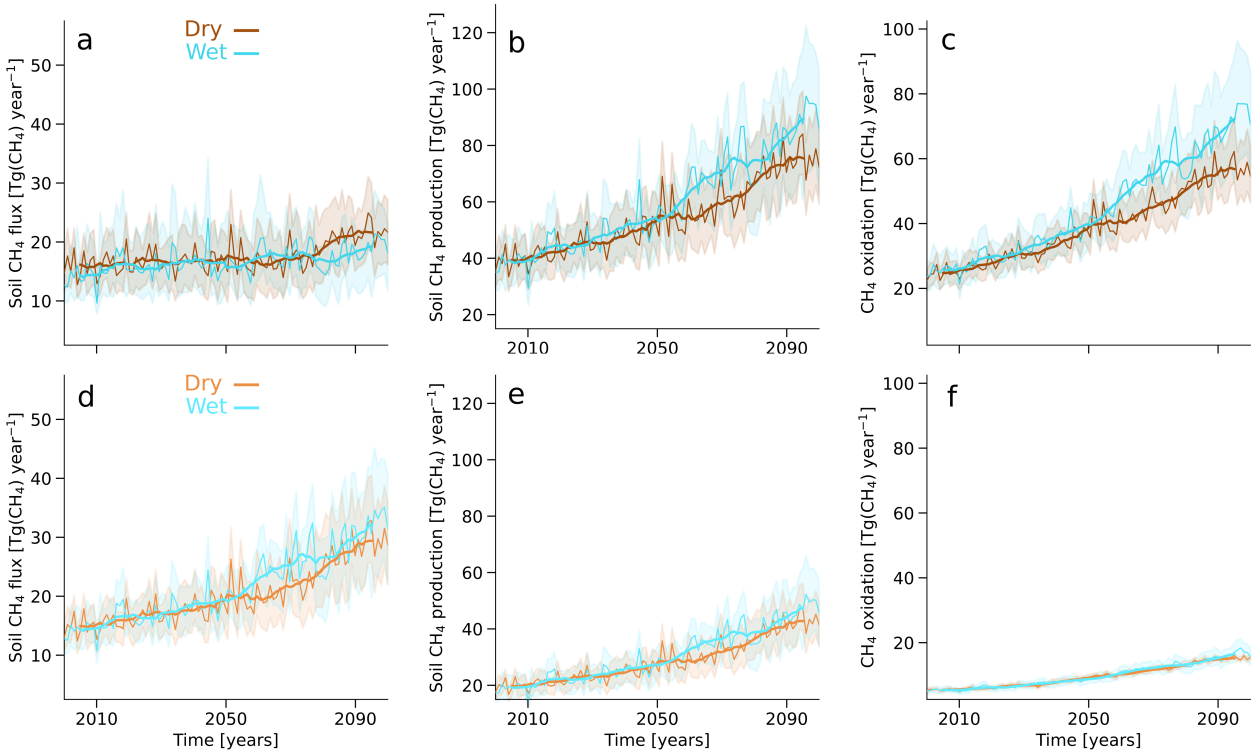

Supplementary Figure SF8. Sources of uncertainty: Methane production and oxidation and plant mediated transport a) Simulated methane release from Arctic soils. Lines show the mean of the ensemble of Wet and Dry JSBACH simulations, with thick lines indicating the 10-year running means. The shaded areas show the spread between the ensemble minima and maxima. b) Same as a but for methane production and c) methane oxidation in methane-producing soils. Subfigures a - c show the high-production-high-oxidation simulations (simulations #3-22 in table ST2). d) - f) Same as a - c, but for the set of low-production-low-oxidation simulations, which also assume a reduced plant mediated transport (simulations #23-42 in table ST2).

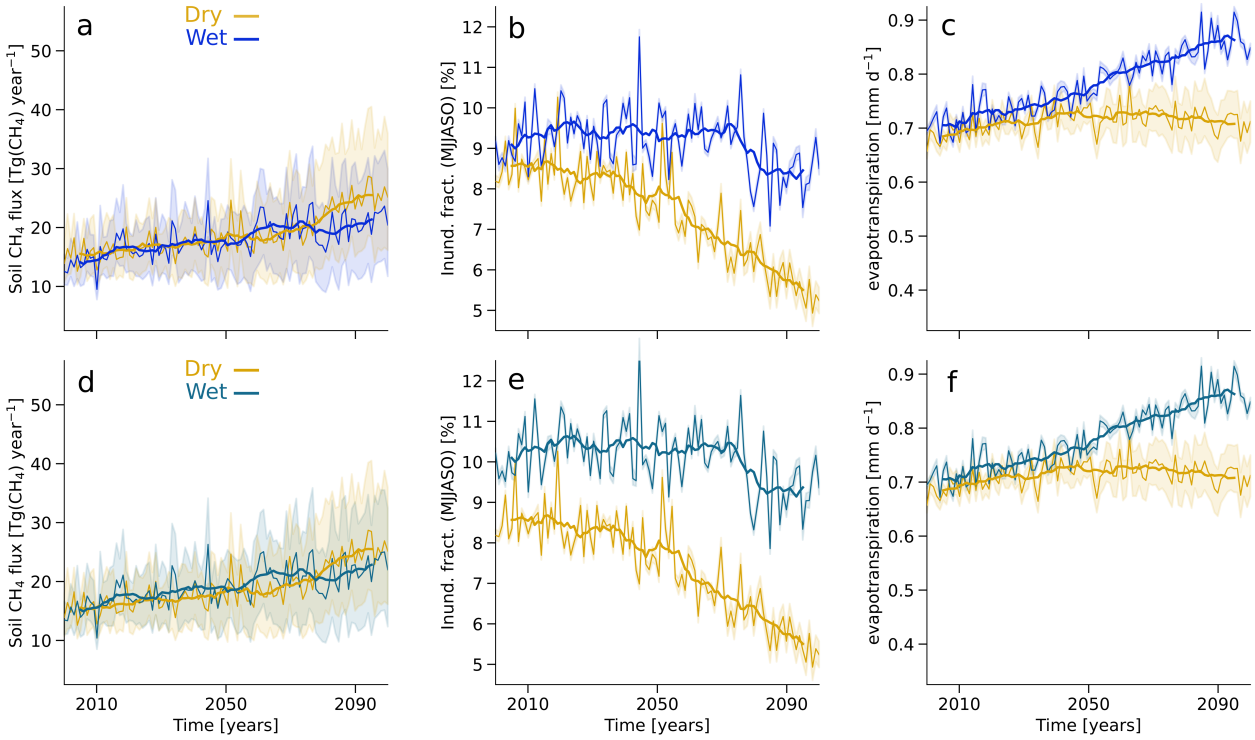

Supplementary Figure SF9. Sources of uncertainty: Wetland area in the Wet scenario I
a) Simulated methane release from Arctic soils. Lines show the mean of the ensemble of Wet and Dry JSBACH simulations, with thick lines indicating the 10-year running means. The shaded areas show the spread between the ensemble minima and maxima. b) Same as a but for the May-October extent of waterlogged areas and c) evapotranspiration. Subfigures a - c show simulations with the physical setup corresponding to the fully coupled MPI-ESM simulations with wet and increasingly dry soils (simulations #3-10 and #23-30 in table ST2). d) - f) Same as a - c, but with the setting of the Wet simulations adding the wetland area of the two wetland components (TOPMODEL-based estimate and the estimate using the WEtland Extent Dynamics scheme; simulations #3-6,#23-26,#11-14 and #31-34 in table ST2).

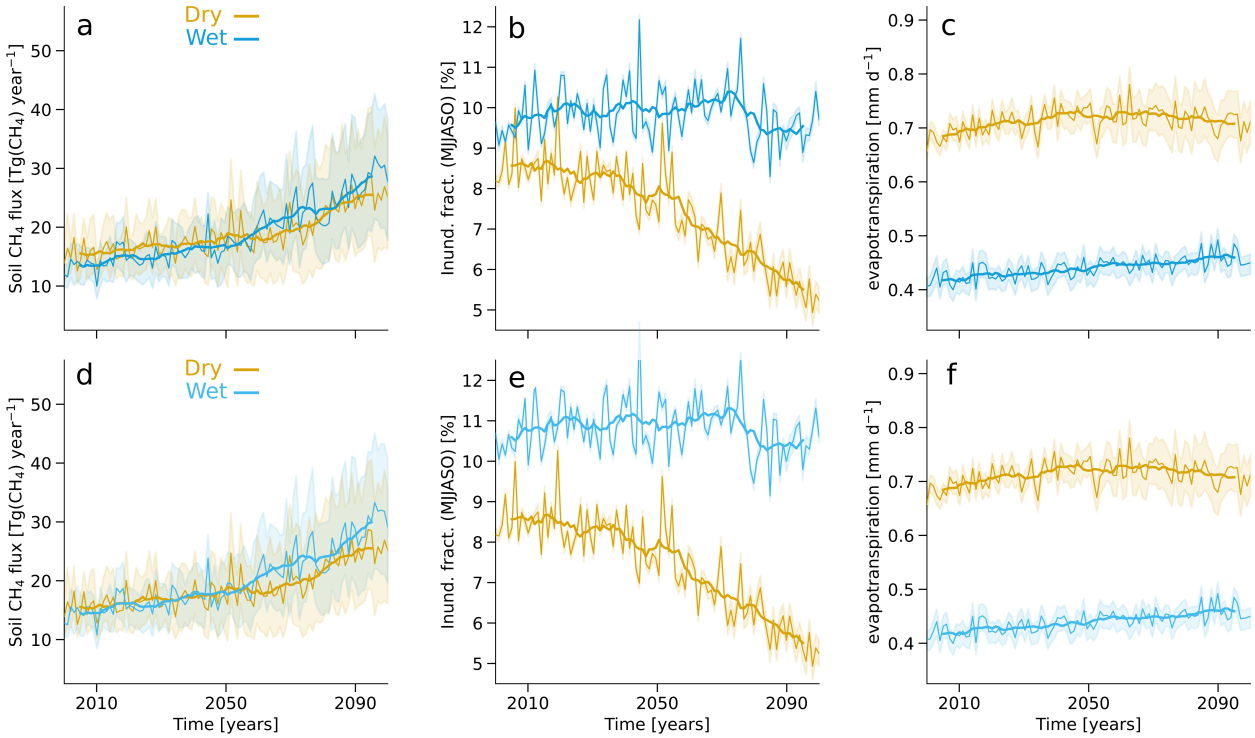

Supplementary Figure SF10. Sources of uncertainty: Wetland area in the Wet scenario II
a - c) Same as Fig. SF9, but the Wet simulations using idealized setup in which the calculation of the evaporative cooling – that is the latent heat flux in the surface energy balance – is based on low resistances, while the amount of evaporated and transpired water is estimated based on a high resistance (simulations #3-6,#23-26,#15-18 and #35-38 table ST2). j) - l) Same as a - c, but for Wet simulations that combine the two approaches to maximize the wetland area – that is adding the grid-cell fractions of the two wetland components rather than taking the maximum of the two and using different assumptions for the calculation of evapotranspiration and the latent heat flux (simulations #3-6,#23-26,#19-22 and #39-42 in table ST2).

Supplementary References

1. de Vrese, P. *et al.* Representation of soil hydrology in permafrost regions may explain large part of inter-model spread in simulated arctic and subarctic climate. *The Cryosphere* **17**, 2095–2118 (2023). URL https://tc.copernicus.org/articles/17/2095/2023/.

2. Hugelius, G. *et al.* Estimated stocks of circumpolar permafrost carbon with quantified uncertainty ranges and identified data gaps. *Biogeosciences* **11**, 6573–6593 (2014). URL https://doi.org/10.5194/bg-11-6573-2014.

3. van Vuuren, D. P. *et al.* The representative concentration pathways: an overview. *Climatic Change* **109**, 5–31 (2011). URL http://dx.doi.org/10.1007/s10584-011-0148-z.

4. Eyring, V. *et al.* Overview of the coupled model intercomparison project phase 6 (CMIP6) experimental design and organization. *Geoscientific Model Development* **9**, 1937–1958 (2016). URL https://doi.org/10.5194/gmd-9-1937-2016.

5. de Vrese, P., Stacke, T., Kleinen, T. & Brovkin, V. Diverging responses of high-latitude co2 and ch4 emissions in idealized climate change scenarios. *The Cryosphere* **15**, 1097–1130 (2021). URL https://doi.org/10.5194/tc-15-1097-2021.

6. Saunois, M. *et al.* The global methane budget 2000–2017. *Earth System Science Data* **12**, 1561–1623 (2020). URL https://doi.org/10.5194/essd-12-1561-2020.

7. Parida, B. The influence of plant nitrogen availability on the global carbon cycle and n2o emissions (2011). URL http://pubman.mpdl.mpg.de/pubman/item/escidoc:1231555.

8. Goll, D. S. *et al.* Carbon–nitrogen interactions in idealized simulations with jsbach (version 3.10). *Geoscientific Model Development* **10**, 2009–2030 (2017). URL https://www.geosci-model-dev.net/10/2009/2017/.

9. Thornton, P. E., Lamarque, J.-F., Rosenbloom, N. A. & Mahowald, N. M. Influence of carbon-nitrogen cycle coupling on land model response to COsub2/subfertilization and climate variability. *Global Biogeochemical Cycles* **21**, n/a–n/a (2007). URL https://doi.org/10.1029/2006gb002868.

10. Cleveland, C. C. *et al.* Global patterns of terrestrial biological nitrogen (nsub2/sub) fixation in natural ecosystems. *Global Biogeochemical Cycles* **13**, 623–645 (1999). URL https://doi.org/10.1029/1999gb900014.

11. Meixner, T. & Bales, R. C. *Biogeochemistry* **62**, 289–308 (2003). URL https://doi.org/10.1023/a:1021118922787.

12. Wang, Y. P., Law, R. M. & Pak, B. A global model of carbon, nitrogen and phosphorus cycles for the terrestrial biosphere. *Biogeosciences* **7**, 2261–2282 (2010). URL https://doi.org/10.5194/bg-7-2261-2010.

13. Hedin, L. O., Armesto, J. J. & Johnson, A. H. Patterns of nutrient loss from unpolluted, old-growth temperate forests: Evaluation of biogeochemical theory. *Ecology* **76**, 493–509 (1995). URL https://doi.org/10.2307/1941208.

14. Koven, C. D., Lawrence, D. M. & Riley, W. J. Permafrost carbon-climate feedback is sensitive to deep soil carbon decomposability but not deep soil nitrogen dynamics. *Proceedings of the National Academy of Sciences* 201415123 (2015). URL https://doi.org/10.1073/pnas.1415123112.

15. von Bloh, W. *et al.* Implementing the nitrogen cycle into the dynamic global vegetation, hydrology, and crop growth model LPJmL (version 5.0). *Geoscientific Model Development* **11**, 2789–2812 (2018). URL https://doi.org/10.5194/gmd-11-2789-2018.

16. Du, E. *et al.* Global patterns of terrestrial nitrogen and phosphorus limitation. *Nature Geoscience* **13**, 221–226 (2020). URL https://doi.org/10.1038/s41561-019-0530-4.

17. Zimov, S. A. *et al.* Permafrost carbon: Stock and decomposability of a globally significant carbon pool. *Geophysical Research Letters* **33** (2006). URL https://doi.org/10.1029/2006gl027484.

18. Zimov, S. A., Schuur, E. A. G. & Chapin, F. S. Permafrost and the global carbon budget. *Science* **312**, 1612–1613 (2006). URL https://doi.org/10.1126/science.1128908.

19. Schuur, E. A. G. *et al.* Vulnerability of permafrost carbon to climate change: Implications for the global carbon cycle. *BioScience* **58**, 701–714 (2008). URL https://doi.org/10.1641/b580807.

20. Batjes, N. Harmonized soil property values for broad-scale modelling (WISE30sec) with estimates of global soil carbon stocks. *Geoderma* **269**, 61–68 (2016). URL https://doi.org/10.1016/j.geoderma.2016.01.034.

21. Batjes, N. H. Harmonized soil profile data for applications at global and continental scales: updates to the WISE database. *Soil Use and Management* **25**, 124–127 (2009). URL https://doi.org/10.1111/j.1475-2743.2009.00202.x.

22. Hagemann, S., Göttel, H., Jacob, D., Lorenz, P. & Roeckner, E. Improved regional scale processes reflected in projected hydrological changes over large European catchments. *Clim. Dyn.* **32**, 767–781 (2009).

23. Hagemann, S. & Stacke, T. Impact of the soil hydrology scheme on simulated soil moisture memory. *Climate Dynamics* **44**, 1731–1750 (2015). URL https://doi.org/10.1007/s00382-014-2221-6.

24. Carvalhais, N. *et al.* Global covariation of carbon turnover times with climate in terrestrial ecosystems. *Nature* **514**, 213–217 (2014). URL https://doi.org/10.1038/nature13731.

25. von Deimling, T. S. *et al.* Long-term deglacial permafrost carbon dynamics in MPI-ESM. *Climate of the Past* **14**, 2011–2036 (2018). URL https://doi.org/10.5194/cp-14-2011-2018.

26. Riley, W. J. *et al.* Barriers to predicting changes in global terrestrial methane fluxes: analyses using CLM4me, a methane biogeochemistry model integrated in CESM. *Biogeosciences* **8**, 1925–1953 (2011). URL https://doi.org/10.5194/bg-8-1925-2011.

27. Kleinen, T., Mikolajewicz, U. & Brovkin, V. Terrestrial methane emissions from the last glacial maximum to the preindustrial period. *Climate of the Past* **16**, 575–595 (2020). URL https://doi.org/10.5194/cp-16-575-2020.

28. Reick, C. H., Raddatz, T., Brovkin, V. & Gayler, V. Representation of natural and anthropogenic land cover change in MPI-ESM. *Journal of Advances in Modeling Earth Systems* **5**, 459–482 (2013). URL https://doi.org/10.1002/jame.20022.

29. Lasslop, G., Brovkin, V., Reick, C. H., Bathiany, S. & Kloster, S. Multiple stable states of tree cover in a global land surface model due to a fire-vegetation feedback. *Geophysical Research Letters* **43**, 6324–6331 (2016). URL https://doi.org/10.1002/2016gl069365.

30. Flannigan, M. *et al.* Global wildland fire season severity in the 21st century. *Forest Ecology and Management* **294**, 54–61 (2013). URL https://doi.org/10.1016/j.foreco.2012.10.022.

31. Senande-Rivera, M., Insua-Costa, D. & Miguez-Macho, G. Spatial and temporal expansion of global wildland fire activity in response to climate change. *Nature Communications* **13** (2022). URL https://doi.org/10.1038/s41467-022-28835-2.

32. BALSHI, M. S. *et al.* Assessing the response of area burned to changing climate in western boreal north america using a multivariate adaptive regression splines (MARS) approach. *Global Change Biology* **15**, 578–600 (2009). URL https://doi.org/10.1111/j.1365-2486.2008.01679.x.

33. Flannigan, M. D., Logan, K. A., Amiro, B. D., Skinner, W. R. & Stocks, B. J. Future area burned in canada. *Climatic Change* **72**, 1–16 (2005). URL https://doi.org/10.1007/s10584-005-5935-y.

34. FLANNIGAN, M., STOCKS, B., TURETSKY, M. & WOTTON, M. Impacts of climate change on fire activity and fire management in the circumboreal forest. *Global Change Biology* **15**, 549–560 (2009). URL https://doi.org/10.1111/j.1365-2486.2008.01660.x.

35. Dai, Y. *et al.* Evaluation of soil thermal conductivity schemes for use in land surface modeling. *Journal of Advances in Modeling Earth Systems* **11**, 3454–3473 (2019). URL https://doi.org/10.1029/2019ms001723.